mathematics

MDPI

Article

Analysis of Jet Wall Flow and Heat Transfer Conveying ZnO-SAE50 Nano Lubricants Saturated in Darcy-Brinkman Porous Medium

Umair Khan [1,2], Aurang Zaib [3], Anuar Ishak [1,*], Iskandar Waini [4], El-Sayed M. Sherif [5] and Ioan Pop [6]

[1] Department of Mathematical Sciences, Faculty of Science and Technology, Universiti Kebangsaan Malaysia (UKM), Bangi 43600, Malaysia
[2] Department of Mathematics and Social Sciences, Sukkur IBA University, Sukkur 65200, Pakistan
[3] Department of Mathematical Sciences, Federal Urdu University of Arts, Science & Technology, Gulshan-e-Iqbal, Karachi 75300, Pakistan
[4] Fakulti Teknologi Kejuruteraan Mekanikal dan Pembuatan, Universiti Teknikal Malaysia Melaka, Hang Tuah Jaya, Durian Tunggal 76100, Malaysia
[5] Mechanical Engineering Department, College of Engineering, King Saud University, Riyadh 11423, Saudi Arabia
[6] Department of Mathematics, Babes-Bolyai University, 400084 Cluj-Napoca, Romania
* Correspondence: anuar_mi@ukm.edu.my

Abstract: The problem of 2D (two-dimensional) wall jet flow, along with heat transfer incorporated by nanofluid in a Darcy-Brinkman medium, while recognizing the requirement for efficient heating and cooling systems. Following the use of similarity variables, the resultant system of ODEs (ordinary differential equations) is solved using the well-known and efficient bvp4c (boundary-value problem of the 4th order) technique. The significance of physical quantities for the under-consideration parameters is illustrated and explained. The findings show that the nanoparticle volume fraction and porosity parameters decrease the velocity, but increase the temperature. In addition, the temperature uplifts in the presence of radiation effect. The suction parameter initially decreases and then increases the velocity near the surface, while the temperature declines.

Keywords: jet wall flow; nanofluid; Glauert model; Darcy-Brinkman porous medium; radiation effect

MSC: 76D05; 76D10; 76D25; 76M20; 76S05

Citation: Khan, U.; Zaib, A.; Ishak, A.; Waini, I.; M. Sherif, E.-S.; Pop, I. Analysis of Jet Wall Flow and Heat Transfer Conveying ZnO-SAE50 Nano Lubricants Saturated in Darcy-Brinkman Porous Medium. *Mathematics* **2022**, *10*, 3201. https://doi.org/10.3390/math10173201

Academic Editors: Wenzhen Qu and Yan Gu

Received: 1 August 2022
Accepted: 29 August 2022
Published: 5 September 2022

1. Introduction

The study of laminar jet flow has drawn the attention of several researchers due to various practical and potential applications, such as the cooling mechanisms for laptops and computers, spray paint drying for automobiles or buildings, cooling jets over components of turbo-machinery, aeroplanes with vertical takeoff and landing spreading out their downward-facing jets across the ground, sluice gate flows, and annealing of plastic and metal sheets, etc. The problems of laminar wall jets can be effectively simplified using the approximation of boundary layer, which is frequently utilized in practice. It was discovered that the related similarity (or non-similarity) results were pertinent for forecasting their performances.

It is now widely acknowledged that Glauert [1] was the first to present the problem of the wall jet created over an impenetrable stationary wall, and to find a solution. According to him, the second similarity restriction relates to a quantity that is the exterior momentum flux, which is rarely interpretable as a physical idea. Riley [2] investigated how a laminar wall jet is affected by mechanical properties. Several scholars, including Merkin and Needham [3,4], expanded Glauert's work to include scenarios in which both wall movement and wall suction or blowing are permitted. They found that, if a traveling wall is included,

the same explanation could only be achieved by applying the proper amount of lateral suction via the moving surface. Magyari and Keller [5] discovered that the connection between suction and the moving wall condition can keep the second similarity restriction proposed by Glauert [1]. Additionally, it was demonstrated by Cohen et al. [6] and Xu et al. [7] that novel types of outcomes are indeed primarily available outside of Glauert's momentum restriction. It should be observed that the innovative outcomes presented by the same researchers, Cohen et al. [8] and Xu et al. [9], as well as those discussed by Magyari and Keller [5], appear to be mathematically vanishing outside of the wall. Several papers [10–12] provide additional analytical and numerical contributions to the study of wall jet flows.

Nanofluids (NFs) are colloidal suspensions of nanometer-sized (up to 100 nm) particles in regular liquid that are differentiated by greater viscosity, according to Choi [13], who coined the term. The thermophysical characteristics of conventional fluids and nanoparticles affect the transport characteristics of the nanofluids. The regular fluid's effective thermal conductivity is increased in the presence of nanoparticles, which improves the features of heat transfer (HT). Singh and Rao [14] used solid lubricants, graphite, and molybdenum disulfide, with an average particle size of the fine powder was around 2 μm, to operate the hard turning of grade steel. The effects of lubricating with graphite and molybdenum disulfide throughout the entire process were investigated, and the outcomes were contrasted with those of machining in a dry cutting environment. In a brilliant review work, Manca et al. [15] demonstrated how different strategies and methodologies, such as increasing the surface of HT or the factor between the surface and the fluid, can improve HT and enable significantly higher rates of heat transfer in a limited volume. Cooling is a significant technical issue that faces several different industries, notably manufacturing, microelectronics, solid-state lighting, and transportation. The thermal conductivity of the final fluids increases when solid metal or metal oxide particles of micrometer or millimeter size are added to the regular fluids. SiO_2 nanoparticles and regular mineral oil were used by Sarhan et al. [16] as a lubricant. They utilized two different methods of lubrication: first, plain mineral oil by itself; and second, incorporation of SiO_2 nanoparticles within the identical mineral oil. It is important to note that Zaidi and Mohyud-Din [17] investigated the effects of MHD (magnetohydrodynamics) and convective heat transfer on a 2D wall jet flow through nanofluid using a model of passive control. The heat transfer features in MHD wall jet flow induced by nanofluids were investigated by Sandeep and Animasaun [18]. Jafarimoghaddam [19] developed the closed-form analytical solution to the mass and heat transfer features of wall jet nanofluid flow by incorporating the mathematical model of nanofluids developed by Buongiorno [20]. Jafarimoghaddam and Pop [21] utilized the Tiwari and Das [22] model of nanofluid to examine the jet flow of exponential decaying type, and presented double solutions. Al-Kouz et al. [23] inspected the three-dimensional MHD flow of water-based CNT/ferroparticles hybrid nanofluid through a wavy walled trapezoidal enclosure with free convection and entropy generation. Recently, Shahzad et al. [24] utilized the neural network to predict the thermal conductivity of nanofluid involving SiC particles.

Darcy's model does not take into account inertia effects or boundaries in porous media, which could affect the flow patterns with heat transfer. Determining the circumstances under which these impacts are significant, is crucial. According to Hong et al. [25], the Brinkman [26] model, which is an elaboration of Darcy's law, should be utilized for no-slip situations. This model was utilized by Ishak et al. [27] to study the steady flow via a vertical surface submerged in a porous media with wall temperature close to the stagnation point. Rosali et al. [28] inspected the buoyancy flow close to a stagnation-point from a vertical plate submerged in a porous media under varying heat flux. The forced convective flow along with heat transport from a plane heated surface saturated in a Darcy-Brinkman porous media was explored by Pantokratoras [29]. Zaib et al. [30] scrutinized the bioconvection flow past a heated wedge with nanofluid in a Darcy-Brinkman porous

medium. Recently, Kausar et al. [31] examined the slip effect on dissipative flow engrossed in a Darcy-Brinkman porous media.

The wall jet has greater technological significance in airfoil design, paint spray, and aircraft take off. The majority of applications utilize turbulent jet flow. In cooling applications, the turbulent state requires the adjustable position of the transition. The nanofluid has additional uses connected to the combustion process and performs well in cooling where there is a wide temperature range. Therefore, the novelty of the problem is to inspect the jet wall flow and heat transfer containing ZnO-SAE50 nanoparticles in a Darcy-Brinkmann porous media, by utilizing the Glauert model. In addition, the radiation influence is also examined. Suitable variables are employed to obtain ordinary differential equations and then find numerical solutions through an efficient bvp4c technique.

2. Formulation of the Model

Consider 2D laminar jet flow of SAE50-ZnO nano-lubricant immersed in a Darcy-Brinkman porous medium with suction/injection and radiation effect, as depicted in Figure 1. The coordinates $x-$ and $y-$ considered along the wall and normal to it, respectively. The temperature of the fluid is signified by T along with the variable wall and ambient temperature $T_w(x)$ and T_∞, respectively. In addition, the thermophysical properties of the nanoparticles and the base fluid are in thermal equilibrium. With these assumptions, the leading equations can be formed as [1–4]

$$\frac{\partial u}{\partial x} + \frac{\partial v}{\partial y} = 0, \tag{1}$$

$$u\frac{\partial u}{\partial x} + v\frac{\partial u}{\partial y} = \frac{\mu_{eff}{\varepsilon_a}^2}{\rho_{nf}}\left(\frac{\partial^2 u}{\partial y^2}\right) - \frac{\mu_{nf}{\varepsilon_a}^2}{K(x)\rho_{nf}}u, \tag{2}$$

$$\left.\begin{aligned} u\tfrac{\partial T}{\partial x} + v\tfrac{\partial T}{\partial y} &= \tfrac{k_{nf}}{(\rho c_p)_{nf}}\left(\tfrac{\partial^2 T}{\partial y^2}\right) - \tfrac{1}{(\rho c_p)_{nf}}\tfrac{\partial q_r}{\partial y}, \\ q_r &= \left(-\tfrac{4\sigma^*}{3k^*}\right)\tfrac{\partial T^4}{\partial y}, T^4 \approx 4T_\infty^3 T - 3T_\infty^4. \end{aligned}\right\} \tag{3}$$

Along with the boundary conditions (BCs)

$$\left.\begin{aligned} u = 0,\ v = v_w(x) = -\sqrt{\alpha_f}x^{-3/4}f_w,\ T = T_w(x)\ \text{ at } y = 0, \\ u \to 0,\ T \to T_\infty \text{ as } \ y \to \infty. \end{aligned}\right\} \tag{4}$$

According to Glauert [1], the subsequent similarity variables and stream function is defined by

$$\xi = \left(\alpha_f^2 x^3\right)^{-1/4} y, \psi = \left(\alpha_f^2 x\right)^{1/4} F(\xi),\ K(x) = K_0\sqrt{x^3} \tag{5}$$

where ψ is the requisite stream function signified as $u = r^{-1}\partial\psi/\partial r$ and $v = -r^{-1}\partial\psi/\partial x$. Hence, the velocity components are derived in the simplified form as

$$u = \frac{4}{\sqrt{x}}F'(\xi), \quad v = -\sqrt{\alpha_f}x^{-3/4}\left(F(\xi) - 3\xi F'(\xi)\right) \tag{6}$$

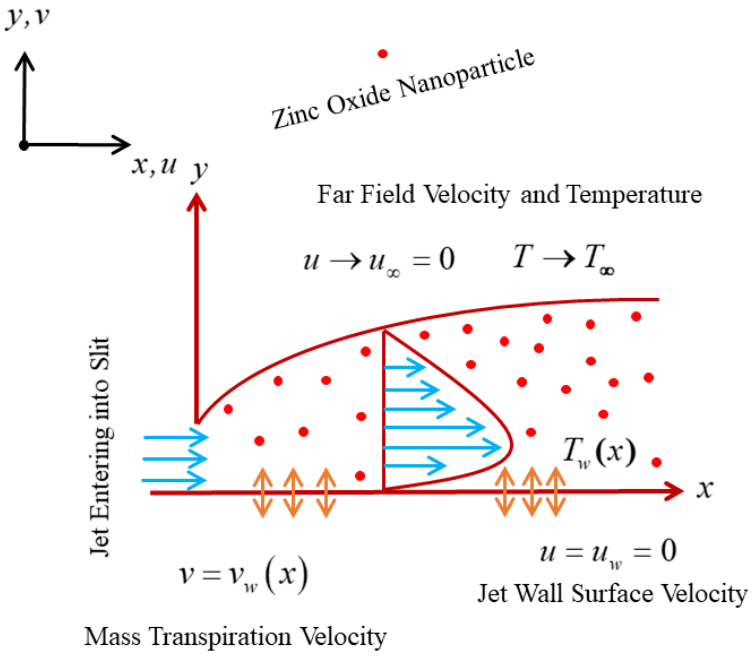

Figure 1. Physical configuration of the jet wall flows and heat transfer embedded nanoparticles.

2.1. For the Momentum Equation

Now, using Equation (5), the continuity equation is satisfied while Equation (2) is reduced to the following form:

$$\frac{\varepsilon_b}{\rho_{nf}/\rho_f}F''' + FF'' + 2F'^2 - \frac{\mu_{nf}/\mu_f}{\rho_{nf}/\rho_f}K_aF' = 0 \tag{7}$$

where $\varepsilon_b = v_{eff}{\varepsilon_a}^2/\alpha_f$, $K_a = v_f{\varepsilon_a}^2/K_0$ are called the dimensionless modified porosity and the dimensionless permeability parameter, respectively.

2.2. For the Energy Equation

Further, Equation (3) can be written in the simplified form as

$$u\frac{\partial T}{\partial x} + v\frac{\partial T}{\partial y} = \frac{k_f}{(\rho c_p)_{nf}}\left(\frac{k_{nf}}{k_f} + \frac{4}{3}R_d\right)\frac{\partial^2 T}{\partial y^2} \tag{8}$$

where $R_d = 4\sigma^* T_\infty^3/k^* k_f$ is called the radiation parameter. To make change the above stated Equation (8) into the posited similarity form, the following variables are introduced:

$$G(\xi) = \frac{T - T_\infty}{T_w(x) - T_\infty}, \quad T_w(x) - T_\infty = T_a x^{\frac{n}{4}} \tag{9}$$

where T_a denotes the usual reference temperature and n is called the temperature index. Also, the energy, Equation (8), is reduced to a similarity form via implementing the above variables (5) and (9). Hence, one obtains

$$\frac{1}{(\rho c_p)_{nf}/(\rho c_p)_f}\left(\frac{k_{nf}}{k_f} + \frac{4}{3}R_d\right)G'' + FG' - nGF' = 0, \tag{10}$$

with BCs are

$$\begin{cases} F(0) = f_w, \ F'(0) = 0, \ G(0) = 1 \ \text{at} \ \xi = 0, \\ F'(\xi) \to 0, \ G(\xi) \to 0 \ \text{as} \ \ \xi \to \infty. \end{cases} \tag{11}$$

In the above BCs, f_w represents the mass transpiration velocity with $f_w > 0$ for suction and $f_w < 0$ for the phenomenon of blowing or injection. Meanwhile, the case $f_w = 0$ represents the impermeable wall jet flow.

2.3. Gradients

In the present study, the following gradients (the shear stress $\left(C_f\right)$ and the heat transfer rate (Nu_x)) are mathematically expressed as:

$$C_f = \frac{1}{\rho_f u_r^2}\left(\mu_{nf}\frac{\partial u}{\partial y}\bigg|_{y=0}\right) \text{ and } Nu_x = \frac{x}{k_f(T_w - T_\infty)}\left(-k_{nf}\frac{\partial T}{\partial y}\bigg|_{y=0} + (q_r)|_{y=0}\right), \quad (12)$$

where μ_{nf} and k_{nf} are the absolute viscosity of the nanofluid and the thermal conductivity of the nanofluid, respectively. Meanwhile, $u_r = 4x^{-1/2}$ corresponds to the reference velocity as taken by Raees et al. [32]. Now, implementing the similarity variables in the above Equation (12), we get

$$2\sqrt{\frac{\mathrm{Re}_x}{\mathrm{Pr}}}C_f = \frac{\mu_{nf}}{\mu_f}F''(0) \text{ and } \frac{2Nu_x}{\sqrt{Pe_x}} = -\left(\frac{k_{nf}}{k_f} + \frac{4}{3}R_d\right)G'(0), \quad (13)$$

where $\mathrm{Re}_x = \frac{u_r x}{\upsilon_f}$, $\mathrm{Pr} = \frac{\upsilon_f}{\alpha_f}$ and $Pe_x = \frac{u_r x}{\alpha_f}$ are called the local Reynolds number, the Prandtl number, and the Peclet number, respectively.

2.4. The Physical Properties of the Nanofluid Model

The mathematical notations used for the nanofluid are absolute viscosity μ_{nf}, thermal conductivity k_{nf}, specific heat capacity $\left(\rho c_p\right)_{nf}$, and density ρ_{nf}. The expression of the thermophysical properties of the NF model can be written as:

$$\frac{\mu_{nf}}{\mu_f} = \frac{1}{(1-\varphi)^{2.5}}, \ \frac{\rho_{nf}}{\rho_f} = \varphi\left(\frac{\rho_{snp}}{\rho_f}\right) + (1-\varphi), \quad (14)$$

$$\frac{k_{nf}}{k_f} = \frac{k_{snp} + 2k_f - 2\varphi\left(k_f - k_{snp}\right)}{k_{snp} + 2k_f + \varphi\left(k_f - k_{snp}\right)}, \quad (15)$$

$$\frac{\left(\rho c_p\right)_{nf}}{\left(\rho c_p\right)_f} = \varphi\left(\frac{\left(\rho c_p\right)_{snp}}{\left(\rho c_p\right)_f}\right) + (1-\varphi). \quad (16)$$

Thus, the above Equations (14)–(16) illustrate the physical features of the ZnO-SAE50 nano lubricant in a nozzle of engine liquid, in which φ implies the nanoparticles' solid volume fraction. Moreover, the subscript snp and f are for the solid nanoparticles and the base working fluid (SAE50), respectively. Generally, the data of the zinc oxide (ZnO) nanoparticles along with the regular base (SAE50) oil fluid are given in Table 1.

Table 1. Experimental physical data of the SAE50 and ZnO [33].

Properties	ρ(kg/m^3)	c_p(J/kgK)	k(W/mK)	μ(Pas)
SAE50	0.906	1900	0.15	0.192543
ZnO	5.606	540	19	-

3. Methodology and Validation of the Scheme

This part of the research work demonstrates the entire mathematical procedure of the scheme, numerical implementation of the scheme, as well as the confirmation of the code. Initially, the wall jet flow and heat transfer problem are bounded in the form of governing

equations. After utilizing the Glauert [1] variables, the governing equations are altered into the similarity ODEs. These ODEs are almost hard to tackle exactly or analytically due to its high non-linearity. Therefore, we have to find the numerical solution of the transformed ODEs (Equations (7), (10), and (11)) for the (SAE50/ZnO) nanofluid flow in a Darcy-Brinkman porous medium by employing an efficient bvp4c technique. The 3-stage Lobatto IIIa formula is implemented using the finite difference algorithm. The considered scheme was documented by Shampine et al. [34] and later so many researchers have followed it, as can be seen from the literature, for example Refs. [35–37]. For the working procedure of the scheme, the higher-order system is transfigured into the first-order ODEs using fresh notations. Let the new variables be

$$F = \Sigma_a, F' = \Sigma_b, F'' = \Sigma_c, G = \Sigma_d, G\prime = \Sigma_e \tag{17}$$

Thus

$$\frac{d}{d\xi}\begin{pmatrix}\Sigma_a\\ \Sigma_b\\ \Sigma_c\\ \Sigma_d\\ \Sigma_e\end{pmatrix} = \begin{pmatrix}\Sigma_b\\ \Sigma_c\\ \frac{\rho_{nf}/\rho_f}{\varepsilon_b}\left(-\Sigma_a\Sigma_c - 2{\Sigma_b}^2 + \frac{\mu_{nf}/\mu_f}{\rho_{nf}/\rho_f}K_a\Sigma_b\right)\\ \Sigma_e\\ \frac{(\rho c_p)_{nf}/(\rho c_p)_f}{\left(k_{nf}/k_f + \frac{4}{3}R_d\right)}(n\Sigma_d\Sigma_b - \Sigma_a\Sigma_e)\end{pmatrix} \tag{18}$$

The boundary conditions become

$$\begin{pmatrix}\Sigma_a(0)\\ \Sigma_b(0)\\ \Sigma_b(\infty)\\ \Sigma_d(0)\\ \Sigma_d(\infty)\end{pmatrix} = \begin{pmatrix}f_w\\ 0\\ 0\\ 1\\ 0\end{pmatrix}. \tag{19}$$

During the simulation process, the code requires initial estimation. It is a single solution problem; therefore, the system requires a suitable or pertinent initial estimation by which the output of the system can hold the convergence criteria and the boundary conditions (19). In addition, we fix the error tolerance $\varepsilon = 10^{-6}$ throughout the computation along with best appropriate finite value of $\xi \to \infty$, such as the thickness of the restricted boundary layer, $\xi = \xi_{\max} = 25$, by which the graphs asymptotically satisfy the criterion of convergence. This procedure is explained in Ref. [38]. Table 2 demonstrates the comparison of the current results with the published work of Glauert [1] and Waini et al. [39] for a special case of the present study. It shows an excellent agreement between these results. Thus, it motivates us and gives confidence that the unavailable outcomes for the impression of several influential parameters are precise or accurate.

Table 2. Numerical assessment of shear stress and heat transfer for several values of n when $f_w = \varphi = K_a = R_d = 0$, and $\varepsilon_b = 1.0$.

n	Glauert [1]	Waini et al. [39]	Present Results	Waini et al. [39]	Present Results
	$F''(0)$	$F''(0)$	$F''(0)$	$-G'(0)$	$-G'(0)$
0.0	$2/9 \approx 0.2222$	0.2222	0.2222	0.6735	0.6735
0.5	-	-	-	0.8193	0.8193
1.0	-	-	-	0.9304	0.9304
1.5	-	-	-	1.0215	1.0215
2.0	-	-	-	1.0993	1.0993

4. Results and Discussion

This section is organized to discuss and basically see the inspiration of the several influential parameters on velocity, temperature, shear stress and heat transfer profiles of the ZnO-SAE50 nano-lubricants. Table 1 presents the thermophysical data of the SAE50 and zinc oxide nanoparticles, while the comparison is shown in Table 2.

Tables 3 and 4 are constructed to inspect the influences of different parameters on the friction factor and the heat transfer rate by utilizing two different methods. The results reveal that the friction factor augments due to φ and ε_b, while it declines due to K_a and f_w. On the other hand, the heat transfer rate enhances due to φ and R_d. Figures 2 and 3 present the impact of φ on the velocity and temperature profiles. The behaviors of these profiles suggest that the velocity declines with increasing φ. This can be attributed to the growing kinetic energy of the nanofluid as its concentration increases; whilst the temperature distribution uplifts due to φ. Physically, it is well-known that φ depends on the nanoparticle's size; therefore, vary in φ impacts the fluids volume's ability to absorb energy.

Table 3. Numerical shear stress values for the several influential parameters.

φ	K_a	ε_b	f_w	$2\sqrt{\frac{\mathrm{Re}_x}{\mathrm{Pr}}}C_f$	$2\sqrt{\frac{\mathrm{Re}_x}{\mathrm{Pr}}}C_f$
				Bvp4c	**RK4**
0.025	0.50	0.70	1.0	1.3200×10^{-9}	1.3200×10^{-9}
0.030	-	-	-	2.4223×10^{-9}	2.4222×10^{-9}
0.035	-	-	-	2.9623×10^{-9}	2.9624×10^{-9}
0.035	0.30	0.70	1.0	3.6085×10^{-9}	3.6085×10^{-9}
-	0.50	-	-	2.9624×10^{-9}	2.9622×10^{-9}
-	0.70	-	-	2.4361×10^{-9}	2.4362×10^{-9}
0.035	0.50	0.60	1.0	1.4477×10^{-9}	1.4476×10^{-9}
-	-	0.65	-	1.8432×10^{-9}	1.8433×10^{-9}
-	-	0.70	-	2.9624×10^{-9}	2.9624×10^{-9}
0.035	0.50	0.70	1.0	2.9624×10^{-9}	2.9624×10^{-9}
-	-	-	1.5	2.2350×10^{-7}	2.2351×10^{-7}
-	-	-	2.0	2.1850×10^{-5}	2.1849×10^{-5}
0.035	0.50	0.70	−0.05	-2.2398×10^{-8}	-2.2398×10^{-8}
-	-	-	−0.10	-1.8970×10^{-8}	-1.8971×10^{-8}
-	-	-	−0.15	-1.5216×10^{-8}	-1.5215×10^{-8}

Table 4. Numerical heat transfer values for the several influential parameters.

φ	n	R_d	$\frac{2Nu_x}{\sqrt{Pe_x}}$	$\frac{2Nu_x}{\sqrt{Pe_x}}$
			Bvp4c	**RK4**
0.025	1.00	2.00	1.0204	1.0204
0.030	-	-	1.0243	1.0244
0.035	-	-	1.0281	1.0282
0.035	0.00	2.00	1.0279	1.0278
-	1.00	-	1.0280	1.0280
-	2.00	-	1.0281	1.0280
0.035	1.00	1.50	1.0273	1.0273
-	-	2.00	1.0280	1.0281
-	-	2.50	1.0302	1.0302

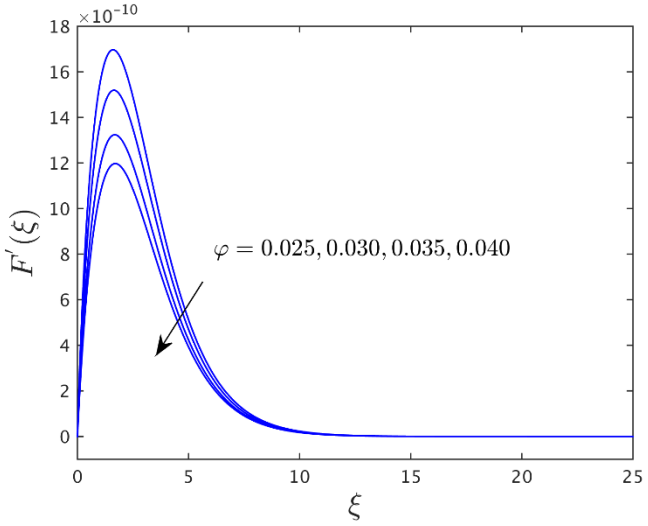

Figure 2. Velocity curves for the distinct values of φ when $n = 1.0$, $K_a = 0.5$, $\varepsilon_b = 0.7$, $f_w = 1.0$, and $R_d = 2.0$.

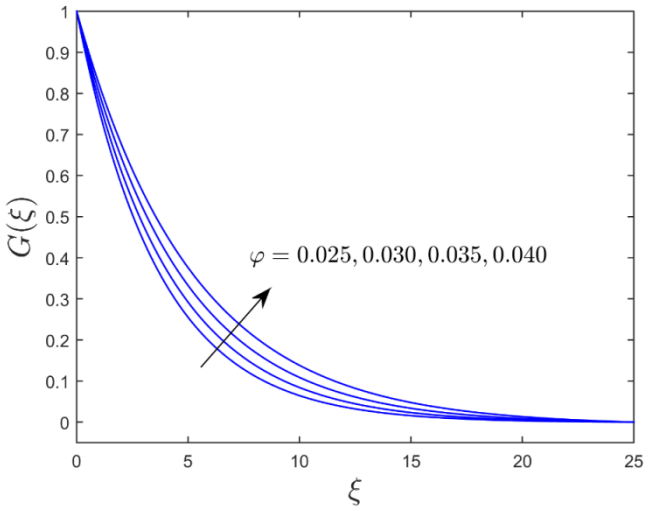

Figure 3. Temperature curves for the distinct values of φ when $n = 1.0$, $K_a = 0.5$, $\varepsilon_b = 0.7$, $f_w = 1.0$, and $R_d = 2.0$.

The impacts of the modified porosity parameter (Brinkman viscosity (BNV)) ε_b are sketched in Figures 4 and 5. The fluid velocity decelerates in the presence of ε_b; whereas the fluid temperature augments due to ε_b. Additionally, this makes sense because, in the momentum equation, the BNV ratio number is paired with the term of velocity gradient, decreasing the velocity as a result of high values of the Brinkman viscosity parameter. Figures 6 and 7 depict the velocity and temperature distributions for some values of the permeability parameter K_a. These results portray that the velocity initially declines and then starts to augment, while temperature also uplifts due to K_a. Physically, the regime gets more porous as the porosity parameter rises, and as a response, the Darcian force's strength moderates. The nanofluid particles slow down due to the resistance produced by the Darcian force. As the porosity parameter rises, this causes the resistance to decrease. The flow suffers reduced drag over time, which reduces flow retardation. The fluid mobility within the boundary layer is therefore enhanced by the porosity characteristic.

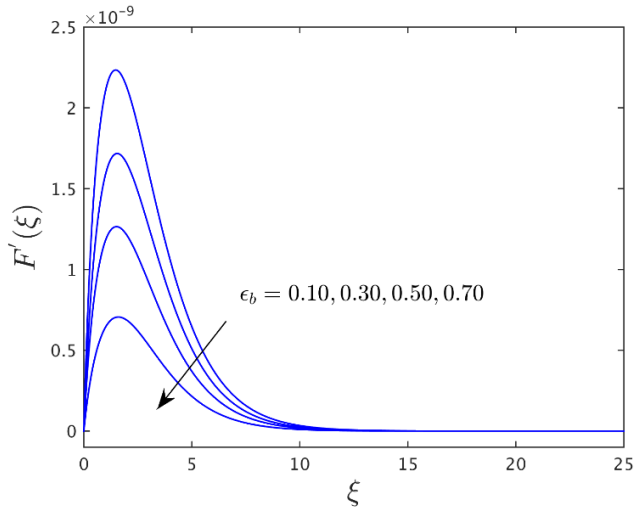

Figure 4. Velocity curves for the distinct values of ε_b when $n = 1.0$, $K_a = 0.5$, $\varphi = 0.035$, $f_w = 1.0$, and $R_d = 2.0$.

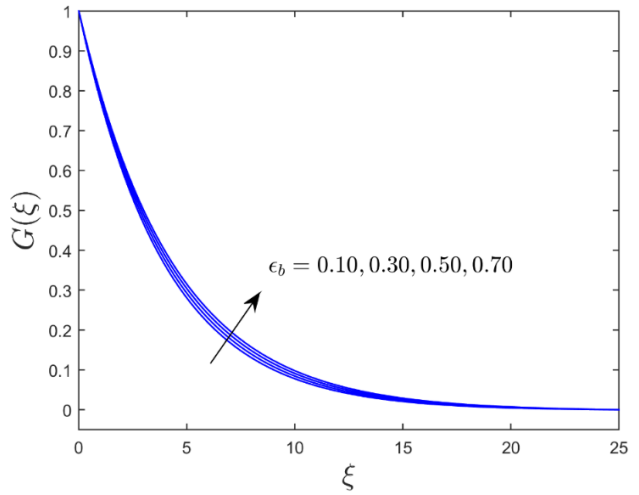

Figure 5. Temperature curves for the distinct values of ε_b when $n = 1.0$, $K_a = 0.5$, $\varphi = 0.035$, $f_w = 1.0$ and $R_d = 2.0$.

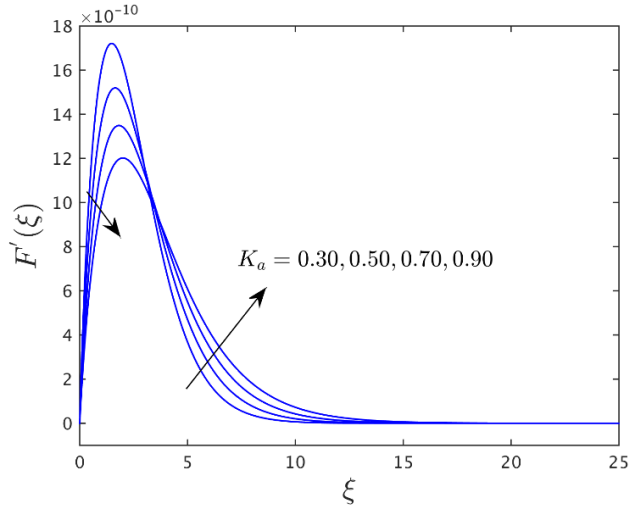

Figure 6. Velocity curves for the distinct values of K_a when $n = 1.0$, $\varepsilon_b = 0.7$, $\varphi = 0.035$, $f_w = 1.0$ and $R_d = 2.0$.

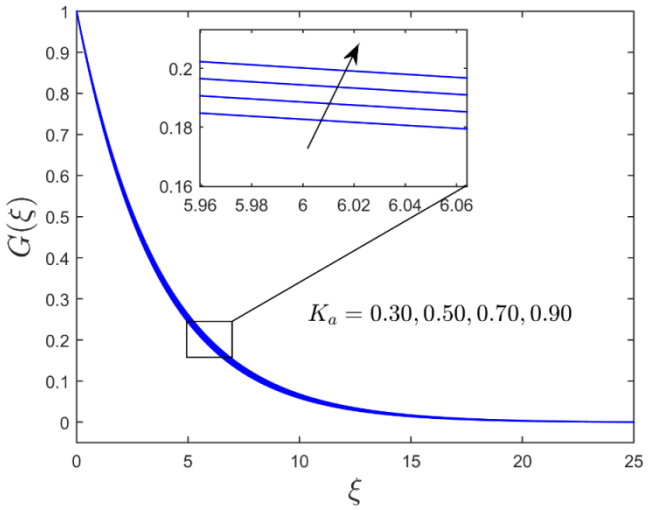

Figure 7. Temperature curves for the distinct values of K_a when $n = 1.0$, $\varepsilon_b = 0.7$, $\varphi = 0.035$, $f_w = 1.0$ and $R_d = 2.0$.

The impression of suction on the velocity and temperature distributions is portrayed, respectively, in Figures 8 and 9. The velocity initially declines and then starts to uplift due to suction. Physically, the stable mass flux decreases drag to prevent flow separation, which consequently increases the jet flow velocity. In contrast, the temperature distribution (see Figure 9) declines with the ramification of suction. The thermal conductivity of the surface slows the flowing molecules due to the surface's permeability, which lowers the jet flow temperature.

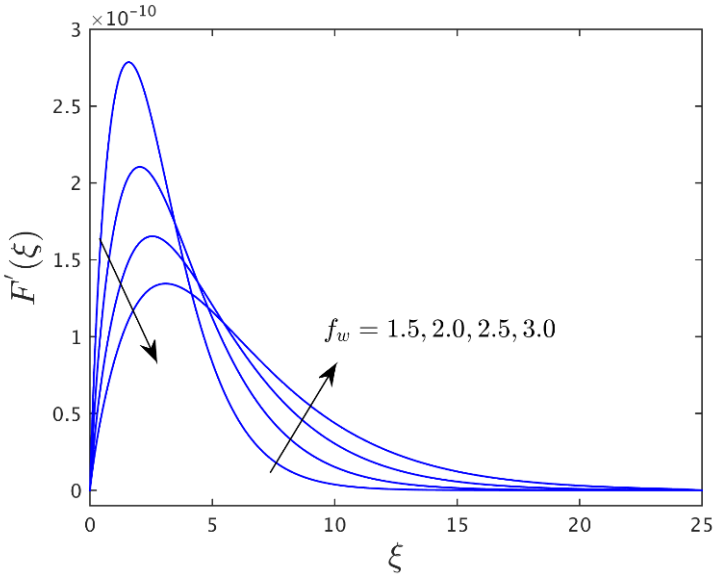

Figure 8. Velocity curves for the distinct values of f_w when $n = 1.0$, $\varepsilon_b = 0.7$, $\varphi = 0.035$, $K_a = 0.5$ and $R_d = 2.0$.

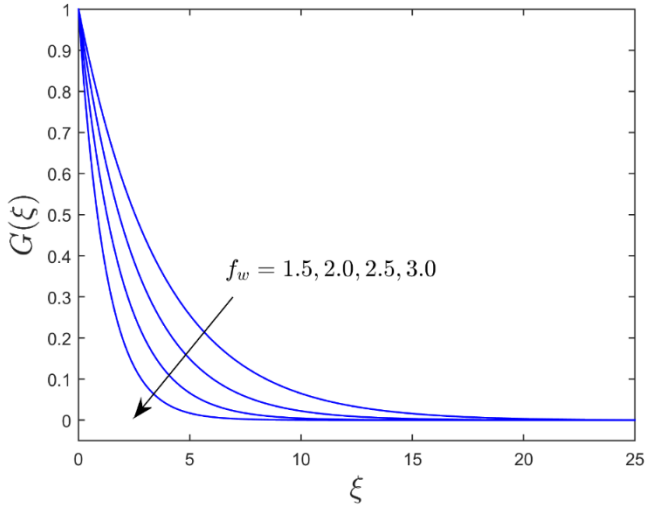

Figure 9. Temperature curves for the distinct values of f_w when $n = 1.0$, $\varepsilon_b = 0.7$, $\varphi = 0.035$, $K_a = 0.5$ and $R_d = 2.0$.

Figure 10 demonstrates the impact of radiation on the temperature distribution. As expected, the temperature of jet flow enhances with radiation effect. Physically, higher radiation level causes the SAE50-ZnO nanoparticles to heat up significantly, raising the jet flow temperature in the meantime. In addition, it increases heat transfer to functioning fluids due to the high radiation effect causes an increase in the thermal boundary layer. When the radiation R_d is increased, the fluid becomes much more heated. As a result, the rate of heat transfer increases noticeably. Moreover, large R_d effectively increases the amount of heat delivered to workable nanofluids, which ultimately increases the temperature.

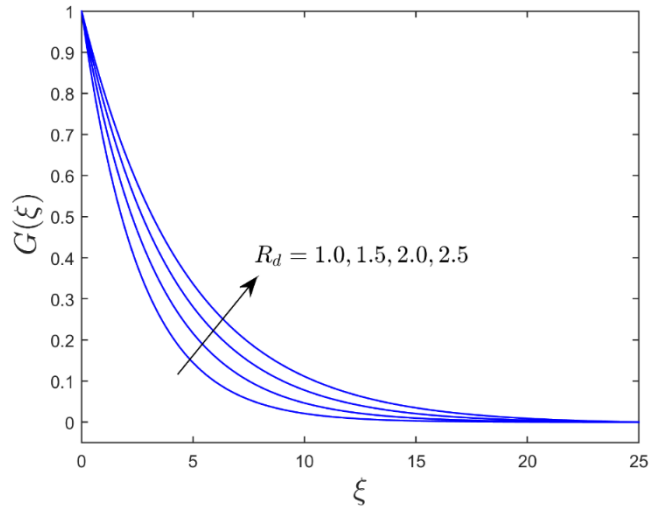

Figure 10. Temperature curves for the distinct values of R_d when $n = 1.0$, $\varepsilon_b = 0.7$, $\varphi = 0.035$, $K_a = 0.5$ and $f_w = 1.0$.

5. Conclusions

In the current exploration, the 2D Glauert wall jet flow incorporates SAE50-based ZnO nanofluid saturated in a Darcy-Brinkman porous medium with radiation and suction effects, was considered. The Glauert variables were utilized to change the leading equations into ODEs and then numerically solved by employing an efficient bvp4c technique. The important findings are summarized as:

➢ The increasing values of φ decline the velocity and improves the heat transfer because of the effective moment of additional heat to the working fluid.

- ➢ The contrary effect is observed on the velocity profile in the presence of porosity and permeability parameters, while the temperature uplifts in the presence of both parameters.
- ➢ The outcomes in both field (velocity and temperature) are asymptotically converging for each influential varying parameter.
- ➢ The radiation impact enhances the jet flow temperature.
- ➢ The suction parameter enhances the jet flow velocity but declines the temperature distribution.

It is worth mentioning that the above work can be further extended by including buoyancy forces or mass transfer with different aspects, such as unsteadiness, shape factors, etc.

Author Contributions: Conceptualization, U.K. and A.Z.; methodology, U.K., A.Z. and I.W.; software, U.K.; validation, E.-S.M.S., U.K., A.I. and I.W.; formal analysis, E.-S.M.S. and A.I.; investigation, U.K.; resources, A.I. and I.P.; data curation, U.K.; writing—original draft preparation, A.Z. and A.I.; writing—review and editing, I.P., E.-S.M.S. and A.I.; visualization, E.-S.M.S. and U.K.; supervision, A.I. and I.P.; project administration, A.I. and I.P.; funding acquisition, A.I. All authors have read and agreed to the published version of the manuscript.

Funding: The given research work was funded by the Universiti Kebangsaan Malaysia (Project Code: DIP-2020-001). Also, this work was funded by the Researchers Supporting Project Number (RSP-2021/33), King Saud University, Riyadh, Saudi Arabia.

Institutional Review Board Statement: Not applicable.

Informed Consent Statement: Not applicable.

Data Availability Statement: Did not report any data.

Acknowledgments: This study was supported by Universiti Kebangsaan Malaysia (Project Code: DIP-2020-001). Also, this research was supported by Researchers Supporting Project Number (RSP-2021/33), King Saud University, Riyadh, Saudi Arabia.

Conflicts of Interest: The authors declare no conflict of interest.

Abbreviations

The following abbreviations are used in this manuscript:

Nomenclature

C_f	Coefficient of skin friction
(x, y)	Cartesian coordinates (m)
$G(\xi)$	Dimensionless temperature
f	Dimensionless velocity
K_a	Dimensionless permeability parameter
T_∞	Free stream constant temperature (K)
Re_x	Local Reynolds number
Nu_x	Local Nusselt number
k^*	Mean absorption coefficient (m^{-1})
f_w	Mass suction parameter
Pr	Prandtl number
K	Permeability of the porous medium (m s)
Pe_x	Péclet number
R_d	Radiation parameter
q_r	Radiative heat flux
c_p	Specific heat at constant pressure (J kg^{-1} K^{-1})
k	Thermal conductivity (Wm^{-1} K^{-1})
T	Temperature (K)
(u, v)	Velocity components in $x-$ and $y-$ axes directions (m s^{-1})
q_w	Wall heat flux
$v_w(x)$	Wall mass velocity (m s^{-1})

Greek symbols	
μ_{eff}	Apparent effective viscosity (kg m^{-1} s^{-1})
μ	Absolute viscosity (kg m^{-1} s^{-1})
ρ	Density (kg m^{-3})
ν_f	Kinematic viscosity (m^2 s^{-1})
ε_b	Modified porosity
ε_a	Porosity parameter
ξ	Pesudo-similarity variable
σ^*	Stefan–Boltzmann constant (W m^{-2} K^{-4})
ψ	Stream function (m^2 s^{-1})
α^*	Thermal diffusivity (m^2 s^{-1})
τ_w	Wall shear stress (kg m^{-1} s^{-2})
Acronyms	
BL	Boundary layer
bvp4c	Boundary value problem of fourth-order
HT	Heat Transfer
MHD	Magnetohydrodynamics
ODEs	Ordinary differential equations
PDEs	Partial differential equations
2D	Two-dimensional
Subscripts	
f	Base fluid
w	Condition at surface
∞	Free-stream condition
nf	Nanofluid
Superscript	
$'$	Differentiation with respect to ξ

References

1. Glauert, M.B. The wall jet. *J. Fluid Mech.* **1956**, *1*, 625–643. [CrossRef]
2. Riley, N. Effects of compressibility on a laminar wall jet. *J. Fluid Mech.* **1958**, *4*, 615–628. [CrossRef]
3. Merkin, J.H.; Needham, D.J. A note on the wall-jet problem. *J. Eng. Math.* **1986**, *20*, 21–26. [CrossRef]
4. Merkin, J.H.; Needham, D.J. A note on the wall-jet problem II. *J. Eng. Math.* **1987**, *21*, 17–22.
5. Magyari, E.; Keller, B. The wall jet as a limiting case of a boundary layer flow induced by apermeable stretching surface. *Z. Für Angew. Math. Phys.* **2001**, *52*, 696–703. [CrossRef]
6. Magyari, E.; Keller, B. The algebraically decaying wall jet. *Eur. J. Mech.* **2004**, *23*, 601–605. [CrossRef]
7. Cohen, J.; Amitay, M.; Bayly, B.J. Laminar-turbulent transition of wall jet flows subjected toblowing and suction. *Phys. Fluids* **1992**, *4*, 283–289. [CrossRef]
8. Xu, H.; Liao, S.-J.; Wu, G.-X. A family of new solutions on the wall jet. *Eur. J. Mech. B Fluids* **2008**, *27*, 322–334. [CrossRef]
9. Selimefendigil, F.; Öztop, H.F. Pulsating nanofluids jet impingement cooling of a heated horizontal surface. *Int. J. Heat Mass Transf.* **2014**, *69*, 54–65. [CrossRef]
10. Turkyilmazoglu, M. Flow of nanofluid plane wall jet and heat transfer. *Eur. J. Mech. B Fluids* **2016**, *59*, 18–24. [CrossRef]
11. Zaidi, S.Z.A.; Mohyud-Din, S.T. Analysis of wall jet flow for soret, Dufour and chemical reaction effects in the presence of MHD with uniform suction/injection. *Appl. Therm. Eng.* **2016**, *103*, 971–979. [CrossRef]
12. Jafarimoghaddam, A. Wall jet flows of Glauert type: Heat transfer characteristics and thethermal instabilities in analytic closed forms. *Eur. J. Mech.* **2018**, *71*, 77–91. [CrossRef]
13. Choi, S.U.S. Enhancing thermal conductivity of fluids with nanoparticles. In *1995 ASME International Mechanical Engineering Congress and Exposition, FED 231/MD*; ASME: New York, NY, USA, 1995; Volume 66, pp. 99–105.
14. Singh, D.; Rao, P.V. Performance improvement of hard turning with solid lubricants. *Int. J. Adv. Manuf. Technol.* **2008**, *38*, 529–535.
15. Manca, O.; Jaluria, Y.; Poulikakos, D. Heat transfer in nanofluids. *Adv. Mech. Eng.* **2010**, *2010*, 380826. [CrossRef]
16. Sarhan, A.A.D.; Sayuti, M.; Hamidi, M. Reduction of power and lubricant oil consumption in milling process using a new SiO_2 nano lubrication system. *Int. J. Adv. Manuf. Technol.* **2012**, *63*, 505–512. [CrossRef]
17. Zaidi, A.S.Z.; Mohyud-Din, S.T. Convective heat transfer and MHD effects on two dimensional wall jet flow of a nanofluid with passive control model. *Aerosp. Sci. Technol.* **2016**, *49*, 225–230. [CrossRef]
18. Sandeep, N.; Animasaun, I.L. Heat transfer in wall jet flow of magnetic nanofluids with variable magnetic field. *Alex. Eng. J.* **2017**, *56*, 263–269. [CrossRef]
19. Jafarimoghaddam, A. Closed form analytic solutions to heat and mass transfer characteristic of wall jet flow of nanofluids. *Therm. Sci. Eng. Prog.* **2017**, *4*, 175–184. [CrossRef]

20. Buongiorno, J. Convective transport in nanofluids. *J. Heat Transf.* **2006**, *128*, 240–250. [CrossRef]
21. Jafarimoghaddam, A.; Pop, I. Numerical modeling of Glauert type exponentially decaying wall jet flows of nanofluids using Tiwari and Das' nanofluid model. *Int. J. Numer. Methods Heat Fluid Flow* **2018**, *29*, 1010–1038. [CrossRef]
22. Tiwari, R.K.; Das, M.K. Heat transfer augmentation in a two-sided lid-driven differentially heated square cavity utilizing nanofluids. *Int. J. Heat Mass Transf.* **2007**, *50*, 2002–2018. [CrossRef]
23. Al-Kouz, W.; Abderrahmane, A.; Shamshuddin, M.D.; Younis, O.; Mohammed, S.; Bég, O.A.; Toghraie, D. Heat transfer and entropy generation analysis of water-Fe_3O_4/CNT hybrid magnetic nanofluid flow in a trapezoidal wavy enclosure containing porous media with the Galerkin finite element method. *Eur. Phys. J. Plus* **2021**, *136*, 1184. [CrossRef]
24. Shahzad, R.M.; Fard, H.F.; Mahariq, I.; El Haj Assad, M.; Al Shabi, M. Thermal conductivity prediction of nanofluids containing SiC particles by using artificial neural network. *Proc. SPIE* **2022**, *12090*, 1209007.
25. Hong, J.T.; Yamada, Y.; Tien, C.L. Effects of non-Darcian and non-uniform porosity on vertical plate natural convectionin porous media. *ASME J. Heat Transf.* **1987**, *109*, 356–362. [CrossRef]
26. Brinkman, H.C. On the permeability of media consisting of closely packed porous particles. *Appl. Sci. Res.* **1947**, *1*, 81–86. [CrossRef]
27. Ishak, A.; Nazar, R.; Pop, I. Dual solutions in mixed convection flow near a stagnation point on a vertical surface in a porous medium. *Int. J. Heat Mass Transf.* **2008**, *51*, 1150–1155. [CrossRef]
28. Rosali, H.; Ishak, A.; Pop, I. Mixed convection stagnation-point flow over a vertical plate with prescribed heat flux embedded in a porous medium: Brinkman-Extended Darcy formulation. *Transp. Porous Media* **2011**, *90*, 709–719. [CrossRef]
29. Pantokratoras, A. Forced convection in a Darcy–Brinkman porous medium with a convective thermal boundary condition. *J. Porous Media* **2015**, *18*, 873–878. [CrossRef]
30. Zaib, A.; Rashidi, M.M.; Chamkha, A.J. Flow of nanofluid containing gyrotatic microroganisms over static wedge in Darcy-Brinkmann porous medium with convective boundary condition. *J. Porous Media* **2018**, *21*, 911–928. [CrossRef]
31. Kausar, M.S.; Hassanan, A.; Mamat, M.; Ahmad, B. Boundary layer flow through Darcy–Brinkman porous medium in the presence of slip effects and porous dissipation. *Symmetry* **2019**, *11*, 659. [CrossRef]
32. Raees, A.; Hang, X.; Raees-ul-Haq, M. Explicit solutions of wall jet flow subject to a convective boundary condition. *Bound. Value Probl.* **2014**, *2014*, 163. [CrossRef]
33. Nayak, M.K.; Prakash, J.; Tripathi, D.; Pandey, V.S. 3D radiative convective flow of ZnO-SAE50 nano-lubricant in presence of varying magnetic field and heterogeneous reactions. *Propuls. Power Res.* **2019**, *8*, 339–350. [CrossRef]
34. Shampine, L.F.; Gladwell, I.; Thompson, S. *Solving ODEs with Matlab*; Cambridge University Press: Cambridge, UK, 2003.
35. Chu, Y.-M.; Khan, U.; Shafiq, A.; Zaib, A. Numerical simulations of time-dependent micro-rotation blood flow induced by a curved moving surface through conduction of gold particles with non-uniform heat sink/source. *Arab. J. Sci. Eng.* **2021**, *46*, 2413–2427. [CrossRef]
36. Hairer, E.; Lubich, C.; Roche, M. *The Numerical Solution of Differential-Algebraic Systems by Runge-Kutta Methods*; Springer: Berlin/Heidelberg, Germany, 2006; Volume 1409.
37. Drąg, M. Numerical infeasibilities of nanofibrous mats process design. *Appl. Sci.* **2021**, *11*, 11488. [CrossRef]
38. Khan, U.; Zaib, A.; Ishak, A.; Bakar, S.A.; Sherif, E.S.M.; Muhammad, N. Radiation effect on three-dimensional stagnation point flow involving copper-aqueous titania hybrid nanofluid induced by a non-Fourier heat flux over a horizontal plane surface. *Phys. Scr.* **2022**, *97*, 015002. [CrossRef]
39. Waini, I.; Ishak, A.; Pop, I. MHD Glauert flow of a hybrid nanofluid with heat transfer. *J. Adv. Res. Fluid Mech. Therm. Sci.* **2021**, *86*, 91–100. [CrossRef]